Journal of Orthopaedic Translation 40 (2023) 104–115

Contents lists available at ScienceDirect

Journal of Orthopaedic Translation

journal homepage: www.journals.elsevier.com/journal-of-orthopaedic-translation

Original Article

Stress stimulation maintaining by genipin crosslinked hydrogel promotes annulus fibrosus healing

Zihan Wang [a,1], Xiaoyu Jin [a,1], Botao Zhang [a], Jiaxin Kong [a], Rongrong Deng [a], Ke Wu [a], Lin Xie [a], Xin Liu [a,**], Ran Kang [a,b,*]

[a] The Third Clinical Medical College, Affiliated Hospital of Integrated Traditional Chinese and Western Medicine, Nanjing University of Chinese Medicine, Nanjing, Jiangsu Province, 210028, PR China
[b] Department of Orthopedics, Nanjing Lishui Hospital of Traditional Chinese Medicine, Nanjing, Jiangsu Province, 210028, PR China

ARTICLE INFO

Keywords:
Stress stimulation
Annulus fibrosus
Genipin crosslinking
Hydrogel
Mesenchymal stromal cells (MSCs)
RhoA/ROCK

ABSTRACT

Objective: To explore the repair effect of tissue engineering for annulus fibrosus (AF) injury in stress-stimulation environment.

Methods: Non-adhesive fibrinogen (Fib) representing the repair with non-stress stimulation and adhesive hydrogel of fibrinogen, thrombin and genipin mixture (Fib-T-G) representing the repair with stress stimulation were prepared to repair the AF lesion. The relationship between adhesion and stress stimulation was studied in rheological measurements, tension tests and atomic force microscopy (AFM) experiments. The repair effect of stress stimulation was studied in designed acellular AF scaffold models with fissures and defects. The models were repaired by the two different hydrogels, then implanted subcutaneously and cultured for 21 d in rats. Histology and qPCR of COL1A1, COL2A1, aggrecan, RhoA, and ROCK of the tissue engineering of the interface were evaluated afterward. Moreover, the repair effect was also studied in an AF fissure model in caudal disc of rats by the two different hydrogels. Discs were harvested after 21 d, and the disc degeneration score and AF healing quality were evaluated by histology.

Result: In interfacial stress experiment, Fib-T-G hydrogel showed greater viscosity than Fib hydrogel (24.67 ± 1.007 vs 459333 ± 169205 mPa s). Representative force-displacement and sample modulus for each group demonstrate that Fib-T-G group significantly increased the interfacial stress level and enhanced the modulus of samples, compared with Fib group ($P < 0.01$). The Fib-T-G group could better bond the interface to resist the loading strain force with the broken point at 1.11 ± 0.10 N compared to the Fib group at 0.12 ± 0.08 N ($P < 0.01$). Focusing on the interfacial healing in acellular AF scaffold model, compared with Fib + MSCs group, the fissure and defect were connected closely in Fib-T-G + MSCs group ($P < 0.01$). Relative higher gene expression of COL2A1 and RhoA in Fib-T-G + MSCs group than Fib + MSCs group in AF fissure and AF defect model ($P < 0.05$). The immunohistochemistry staining showed more positive staining of COL2A1 and RhoA in Fib-T-G + MSCs group than in Fib + MSCs group in both AF fissure and AF defect models. The degree of disc degeneration was more severe in Fib + MSCs group than Fib-T-G + MSCs group *in vivo* experiment (11.80 ± 1.11 *vs* 7.00 ± 1.76, $P < 0.01$). The dorsal AF defect in Fib-T-G + MSCs group (0.02 ± 0.01 mm^2) was significantly smaller than that (0.13 ± 0.05 mm^2) in Fib + MSCs group ($P < 0.05$). Immunohistochemical staining showed more positive staining of COL2A1 and Aggrecan in Fib-T-G + MSCs group than in Fib + MSCs group.

Conclusion: Genipin crosslinked hydrogel can bond the interface of AF lesions and transfer strain force. Stress stimulation maintained by adhesive hydrogel promotes AF healing.

The translational potential of this article: We believe the effect of stress stimulation could be concluded through this study and provides more ideals in mechanical effects for further research, which is a key technique for repairing intervertebral disc in clinic. The adhesive hydrogel of Fib-T-G + MSCs has low toxicity and helps bond the interface of AF lesion and transfer strain force, having great potential in the repair of AF lesion.

* Corresponding author.
** Corresponding author. The Third Clinical Medical College, Affiliated Hospital of Integrated Traditional Chinese and Western Medicine, Nanjing University of Chinese Medicine, Nanjing, Jiangsu Province, 210028, PR China.
E-mail addresses: liuxin@njucm.edu.cn (X. Liu), kangran126@126.com (R. Kang).
[1] Zihan Wang and Xiaoyu Jin contributed equally to this work.

https://doi.org/10.1016/j.jot.2023.05.010
Received 23 February 2023; Received in revised form 20 April 2023; Accepted 30 May 2023
Available online 12 June 2023

1. Introduction

Annulus fibrosus (AF) is located on the periphery part of the intervertebral disc, preventing the nucleus pulposus (NP) displacement. Lesion of AF is a main pathological factor of NP herniation, which causes symptoms of low back pain and subsequent pathological progress of intervertebral disc degeneration (IVD) and spinal canal narrowing [1]. Therefore repair of AF lesions has priority in disc disease treatment strategy [2].

Suturing is the most direct method to close AF lesions with unexpected poor healing due to the disc's limited self-repair capability and the suture's possible stress occlusion [3] (Fig. 1A). In order to solve the problem of stress occlusion, the hydrogel that can bond the cross-section becomes the appropriate choice. However, the non-adhesive hydrogel has a limited effect because it cannot generate enough stress stimulation to support interface healing (Fig. 1B). An ideal repair method should effectively couple the broken fibers of the ruptured interface to transfer stress stably and also provide proper seed cells to stimulate and promote regeneration (Fig. 1C).

Mesenchymal stromal cells (MSCs) are important seed cells for AF regeneration [4], and their differentiation process is influenced by the mechanical environment [5]. Studies have shown that the RhoA/ROCK signaling pathway is the main pathway for mechanical stimulation to regulate MSCs differentiation [6]. In our previous study, we found that stress stimulation activated RhoA, which promoted MSCs differentiation to produce ordered collagen similar to AF tissue, and thus inferred that stress stimulation might regulate the differentiation of MSCs to AF-like cells through the RhoA/ROCK signaling pathway [7]. Therefore, choosing a suitable material that can adhere to the section tightly and provide a stable stress-stimulating environment for MSCs differentiation is an important direction for promoting AF regeneration.

Lots of biomaterials have been investigated to couple or bridge the ruptured interface [8–10], including adhesive-related materials such as surgical glue [11], genipin [12], alginate, agarose, gelatin, and collagen, and/or together with defect filler made by synthetic polyglycolic acid, polylactic acid, poly ε-caprolactone [13], or made by nature acellular AF [10]. In fact, adhesives with excellent bonding strength and biocompatibility are still under development [14]. Among them, genipin is a biological crosslinking agent extracted from the fruits of gardenia jasminoides and genipin americana [15], with the characteristic of enhancing gel's bonding strength and successfully used in the treatment of cartilage degeneration [16], central neurodegenerative diseases [17] and eyes related diseases [18,19]. This unique natural crosslinker is in favor rather than others [11] because it not only enhances the gel strength to bridge the ruptured interface but also helps to provide a hypertoxicity [20] environment for cell homing, proliferation, and differentiation [21], which is one of the most potential options for repairing AF.

However, there are few reports in the literature about AF repair using hydrogel [12,22], which may be because the adhesive strength is still insufficient to withstand the strong stress from the intervertebral disc of human or animal models. Hence, we designed a unique experimental model of fissure and defect in acellular AF scaffolds, which requires less adhesive strength for repair and gives the possibility to study whether stress stimulation maintained by genipin crosslinked hydrogel promotes AF healing. The adhesive hydrogel of fibrinogen, thrombin and genipin mixed with MSCs (Fib-T-G + MSCs), and the non-adhesive hydrogel of fibrinogen mixed with MSCs (Fib + MSCs) were prepared to repair AF

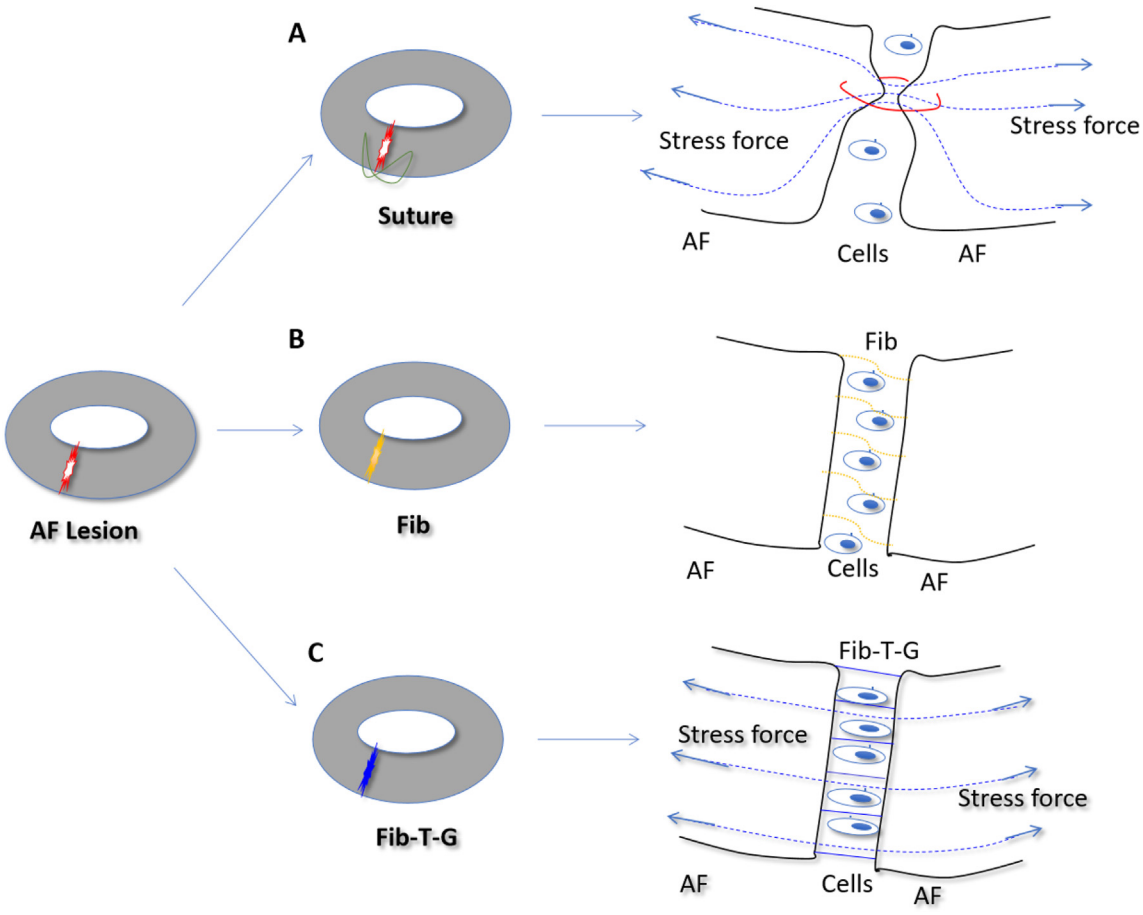

Figure 1. Suturing *vs* fibrin-genipin adhesive hydrogel. Suturing is the most direct method, but stress occlusion of the suture may affect annulus healing. In contrast to Fibrin-genipin non-adhesive hydrogel, Fibrin-genipin adhesive hydrogel could bond the cross section tightly by making the stress transfer evenly.

lesion, representing the repair in stress and non-stress stimulation environment respectively. The repaired models were cultured subcutaneously in rats, where the hydrogel could sufficiently sustain the stress forces from the model's deformation and the rat's daily activities (Fig. 2). Moreover, the repair of AF fissure model in the rat caudal intervertebral disc, where the force is affordable for the hydrogel, is also studied. It is believed that this study can summarize the effect of genipin stress stimulation and provide more ideas for further research in the repair of AF.

2. Experimental section

All animal experiments were performed according to the Guidelines for Care and Use of Laboratory Animals established by the Animal Experiment Ethics Committee of the Affiliated Hospital of Integrated Traditional Chinese and Western Medicine, Nanjing University of Chinese Medicine. The protocol was approved by the Animal Experiment Ethics Committee of the Hospital (Ethical Lot Number: AEWC-20191010-82).

2.1. Fabrication of acellular AF scaffold

Referring to our previous study [10], AF samples harvested from fresh bovine tails were frozen in liquid nitrogen for 22 h prior to thawing in a hypotonic buffer (10 mM tris–HCl, pH 8.0) at 37 °C for 2 h. A 75% ethanol pre-wash of AF samples was then conducted for 2 h. Subsequently, AF samples were placed in the decellularization solution, which consisted of tris–HCl buffer (10 mM Tris–HCl, pH 8.0) containing 0.2% SDS, 0.1% EDTA, and 10 KIU/mL aprotinin at 4 °C for 24 h with gentle agitation (40 r/m) on an orbital shaker. After transient rinsing, samples were submerged in deoxyribonuclease (DNase 50 U/mL; Sigma, USA) and ribonuclease (RNase 1 U/mL; Sigma, USA) in Tris buffer (50 mM tris–HCl, 10 mM magnesium chloride, and 50 mg/mL bovine serum albumin at pH 7.5) for 3 h at 37 °C with gentle agitation. Decellularized AF scaffolds were eventually acquired after being constantly washed three times in PBS for 8 h. Scaffolds were freeze-dried and stored in a sterile environment for further use.

2.2. Preparation of Fib-T-G + MSCs and Fib + MSCs hydrogels

Fib-T-G + MSCs adhesive hydrogel contained final concentrations of 140 mg/mL fibrinogen (F3879, Sigma, USA), 28 U/mL thrombin (T4393, Sigma, USA), and 6 mg/mL genipin (G4796, Sigma, USA) mixed with MSCs (purchased from ScienCell Research Laboratories, Carlsbad, CA) at a concentration of 5×10^4/50 μL, according to previous M. Likhitpanichkul's study [12]. Fib + MSCs adhesive hydrogel contained the same composition but lacked thrombin and genipin. The adhesive hydrogels were prepared in a sterile environment just before application.

2.3. Rheological measurements

Rheological measurements were made using a rotary rheometer (MCR302, Anton Paar) to compare the adhesion of Fib and Fib-T-G hydrogels. The increased shear stress test temperature was set at 25 °C and the shear rate gradually increased to 50 s^{-1}. Viscosity and shear stress were recorded for comparison. Then measurements were carried out at 36 °C and shear rate of 0.04 s^{-1} to compare the viscosity of Fib hydrogel to Fib-T-G hydrogel at a constant shear rate (Fig. 3A and B).

2.4. Tension test

The relationship between stress stimulation and adhesion was measured using the following pioneering method (Fig. 4A and B). AF samples harvested from fresh bovine tails were trimmed in size of 0.8 cm in height, 0.8 cm in width, and 1.6 cm in length, then they were cut in the middle into two equal parts, with direction perpendicular to the fiber. The AF fissure was repaired by three methods: the Suture group was repaired with sutures; the Fib group was repaired by non-adhesive hydrogel of fibrinogen; the Fib-T-G group was repaired by fibrinogen, thrombin and genipin adhesive hydrogel. During the repair process, a strain voltmeter (RK-23, RunesKee) was placed between the fissure to reflect stress changes with voltage. After being wrapped in physiological saline gauze and placed in the incubator at 37 °C for 2 h, the samples were loaded at horizontally placed hand pressure tension test frame (WK-J, WD) by strain force with loading rate of 5 mm/min untile failure, meanwhile the voltage value in the voltmeter representing interfacial strain force was recorded at loading force of 0.1 N, 0.2 N, 0.3 N, 0.4 N.

2.5. Atomic force microscopy (AFM)

Two New Zealand white rabbits (average weight 2.5–3 kg, mature , 6 months of age) were euthanized, and discs between L1 and L7 vertebral bodies were exposed and divided by Fib group and Fib-T-G group (n = 6).

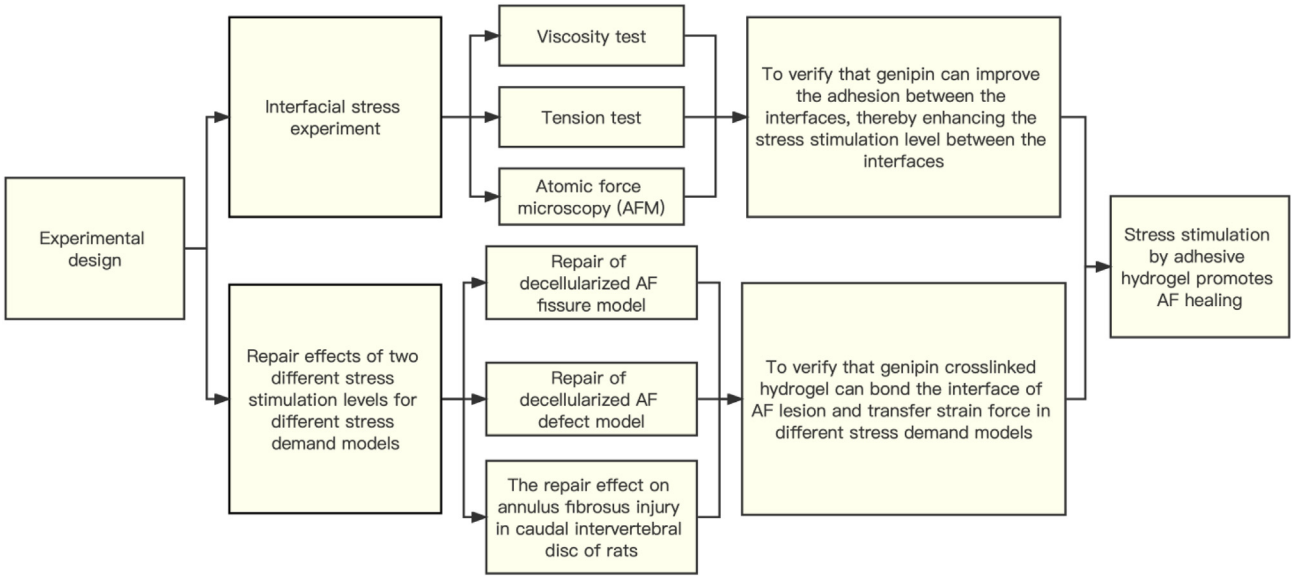

Figure 2. Experimental design.

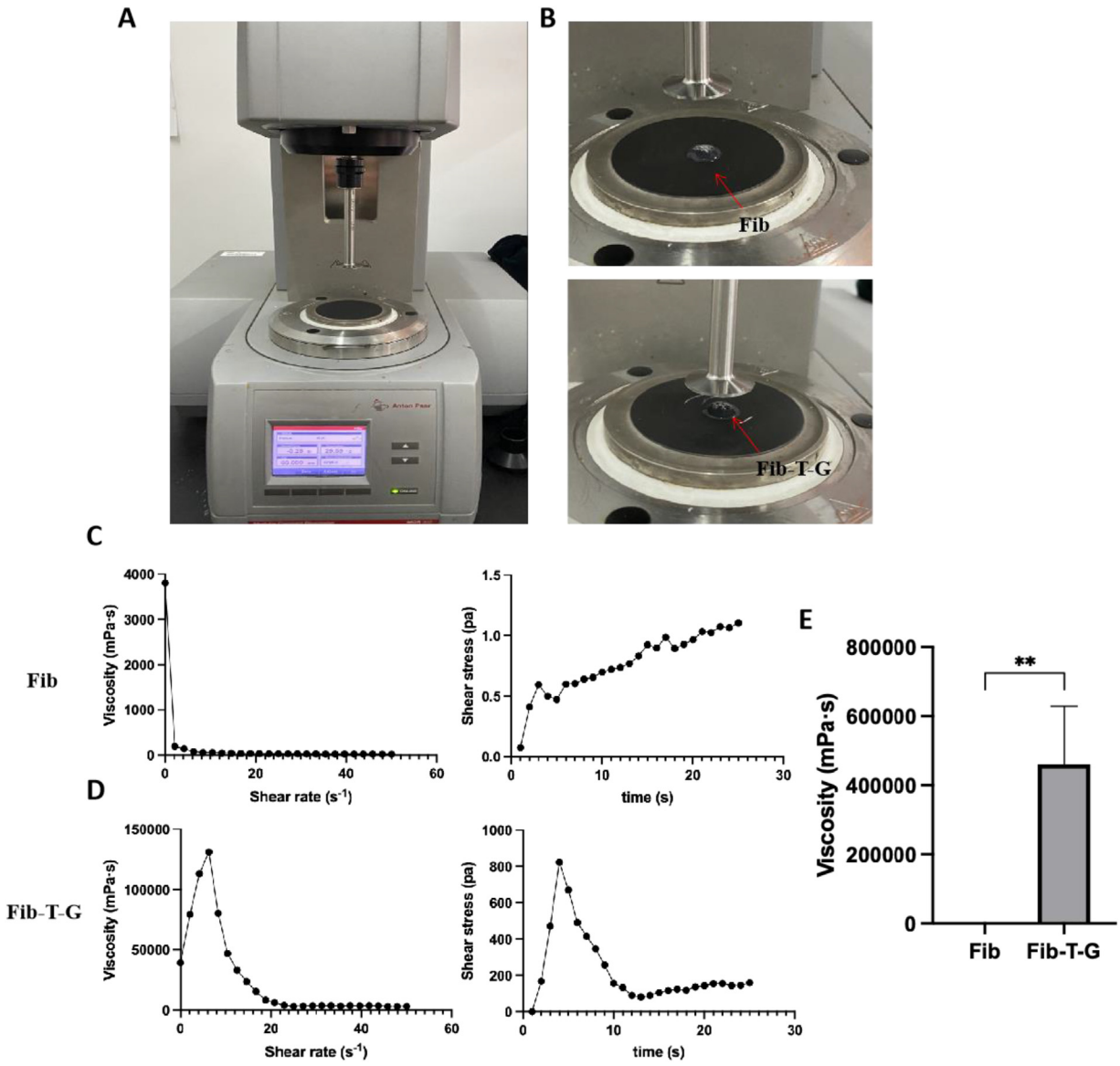

Figure 3. Rheological measurements (A) Rotational rheometer (B) Hydrogel of Fib and Fib-T-G (C) Viscosity and shear stress of Fib hydrogel at 25 °C and gradually increase the shear rate to 50 s-1 (D) Viscosity and shear stress of Fib-T-G hydrogel at 25 °C and gradually increase the shear rate to 50 s-1 (E) Viscosity of Fib and Fib-T-G hydrogels at 36 °C and shear rate of 0.04 s^{-1}.

A 2 mm and 4 mm diameter hole were drilled with a hole punch, followed by Fib and Fib-T-G hydrogel, respectively, to repair the defect (Fig. 5C and D). The samples were placed in medical gauze soaked with PBS and bathed in water at room temperature for 4 h. Motion segments were cryosectioned in the sagittal plane at 20 μm thick using Kawamoto's film method [23]. After thawing in PBS with protease inhibitors, AFM-nanoindentation was performed on defections using microspherical colloidal tips (AC240TM-R3-10, Olympus) using a dimension icon AFM (MFP 3D, America) (Fig. 5E and F). AC tapping mode was introduced to image the corresponding morphologies in the air using a silicon nitride AFM tip with a curvature radius of 7 nm. Force spectroscopy was performed using "closed loop" AFM system with a sensor piezo. Before acquiring force spectroscopy data, the AFM cantilever spring constant was calibrated through the resonance frequency changes, which were induced by small mass. The cantilever spring constant of the tips used in this work was calibrated as 0.1 N/m. The sample's modulus was calculated using the Hertz model, as previously described [24] (Fig. 5A and B).

2.6. Stress stimulation effect study on decellularized AF fissure and defect model

2.6.1. Repair of decellularized AF fissure model

The decellularized AF scaffold cuboid (trimmed in size of 0.6 cm in height, 0.6 cm in width, and 1.5 cm in length) was cut in the middle into two equal parts, with direction across the fibers. The scaffold with the cut was used as decellularized AF fissure model. Twelve models were cross-linked with Fib-T-G + MSCs adhesive hydrogel and sutured by 4–0 nonabsorbable polypropylene suture (SURGI PRO™) (Fig. 6A) as the experimental group. Another twelve models as the control group, cross-linked with Fib + MSCs adhesive hydrogel and sutured similarly. After repair, all the models were wrapped in physiological saline gauze and placed in the incubator at 37 °C for 2 h. Twelve SD rats (average weight 410 ± 26 g, male) were used for subcutaneously culturing the samples, by taking one sample from each group and implanting at each side of rat's shoulder blades behind the ears (Fig. 6A). After 21 d, six samples in each

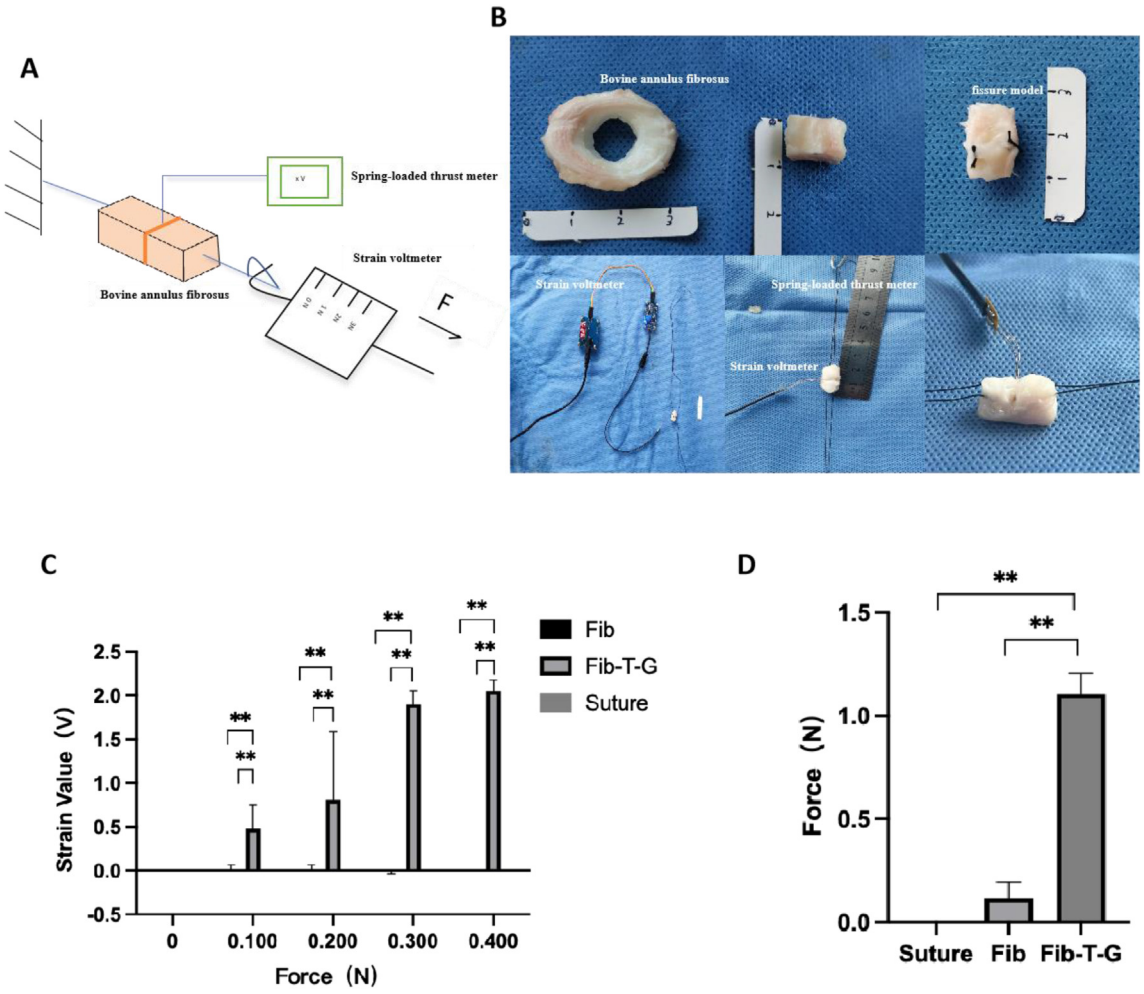

Figure 4. Tension test (A) Diagram of the experiment of interfacial stress in sutures, Fib and Fib-T-G group (B) Construction of fissure model and actual experimental procedure (C) Changes of strain value with differnt forces (D) Maximum breaking force.

group were harvested and fixed in formaldehyde for histological analysis. The other six samples in each group were harvested and immediately stored in liquid nitrogen for further quantitative real-time PCR (qPCR, ABI StepOnePlus, USA) analysis.

2.6.2. *Repair of decellularized AF defect model*

The decellularized AF scaffold cuboid (trimmed in size of 0.6 cm in height, 0.6 cm in width, and 1.5 cm in length) was carved all through AF by a custom-made punch (square opening 3 mm × 3 mm, 6 mm in depth). The scaffold with the hole was used as the decellularized AF defect model. Twelve models were filled and cross-linked with Fib-T-G + MSCs adhesive hydrogel, replanted the punched-out piece of scaffold, then sutured by 4–0 nonabsorbable polypropylene suture (SURGI PROTM) (Fig. 7A) as the experimental group. Another twelve models in the control group were filled and cross-linked with Fib + MSCs adhesive hydrogel, replanted the punched-out piece of scaffold, and sutured the same way. After repair, all the models were wrapped in physiological saline gauze and placed in the incubator at 37 °C for 2 h. Subcutaneously culturing and histological and qPCR analysis were the same as above.

2.6.3. *Histological assay*

Sample sections with 7 μm thickness were stained with Hematoxylin and Eosin staining (HE, Bios Europe, Skelmersdale, UK) and Picrosirius Red staining (ab150681, Abcam, USA). The non-healing area in the fissure or defect was calculated the middle representative section by software (ImageJ 2.3.0) (Figs. 6B and 7B). Immunohistochemistry (IHC) of collagen I (COL1A1) (1:200, ab34710, Abcam, USA), collagen II (COL2A1) (1:200, ab34712, Abcam, USA), aggrecan (1:200, ab36861, Abcam, USA), and mechanical stimulation signal pathway-related protein RhoA (1:100, 10749-1-AP, Proteintech, China) and ROCK (1:200, ab97592, Abcam, USA) was performed. Epitopes were quantified using image analysis software (Image-Pro Plus 6.0). All IHC samples were set as negative control groups. The specific steps are as follows: put the sample slide obtained by paraffin section into sodium citrate (P0083, Beyotime, China) for thermal induction to extract antigen, then put the slide into hydrogen peroxide solution (3%), and incubate it in the dark at room temperature for 25 min to block endogenous peroxidase. Then, the buffer solution (10% normal goat serum and 0.3% Triton X-100 in PBS) was used for infiltration and sealing. Next, the slides were incubated with primary antibodies (COL1A1, COL2A1, aggrecan, RhoA, ROCK) overnight at a 4 °C refrigerator. The slices were washed with PBS (pH7.40, 0.01 M) for 3 times, and after 5 min each time, the slices were co-incubated with the corresponding secondary antibody (HRP conjugated goat anti-mouse, Proteintech, 1:100 dilution) again in the dark at 37 °C for 2 h, followed by DAB (ZLI-9018, ZSGB-BIO, China) chromogenic process. The specific steps were as follows: the sections were placed in PBS solution and washed 3 times in a shaker for 5 min each time. Subsequently, the sections were slightly dried, and the DAB developer solution was added. The color development time was controlled by microscope observation, and the positive color was brown and yellow. Then, the sections were washed with tap water to stop the color development and then were re-stained with hematoxylin. Finally, the sections

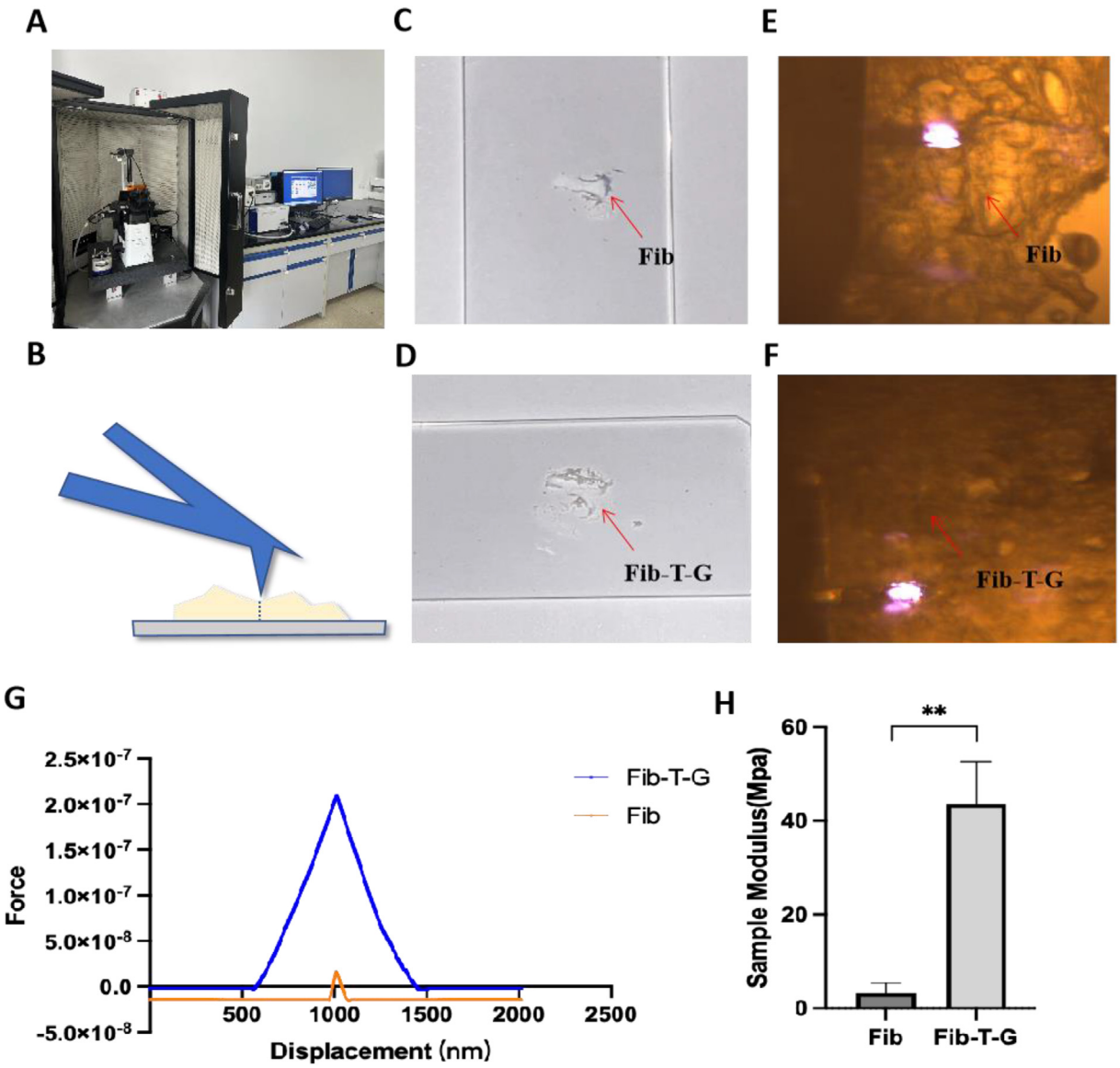

Figure 5. Atomic force microscopy (AFM) (A) Atomic force microscopy (AFM) (B) Diagram of the AFM experiment (C) Freezing microtome section of the defect filled with Fib hydrogel (D) Freezing microtome section of the defect filled with Fib-T-G hydrogel (E) Image of the defect filled with Fib hydrogel under the atomic force microscopy (F) Image of the defect filled with Fib-T-G hydrogel under the atomic force microscopy (G) Force-displacement curves (H) Sample modulus.

were observed under a fluorescence microscope.

2.6.4. qPCR analysis

After incubation for 3 d, the total RNA from samples was isolated using Trizol reagents (15596026, Invitrogen, USA) according to the manufacturer's instructions. The RNA was synthesized by reverse transcription kit (E6560, NEB, USA) to cDNA, followed by qPCR analysis using SYBR Premix (E3003, NEB, USA) and ABI STEPONE PLUS. Gene expression of COL1A1, COL2A1, Aggrecan, RhoA, and ROCK was analyzed by qPCR Glyceraldehyde 3-phosphate dehydrogenase (GAPDH) was used as a reference gene. The sequences of the genes are shown in Table 1.

2.7. Stress stimulation effect study on caudal intervertebral disc AF fissure model in rats

2.7.1. Repair of caudal intervertebral disc AF fissure model in rats

Twenty SD rats (average weight 445 ± 30 g, male) were utilized in this study with 10% chloral hydrate anesthesia. Four caudal intervertebral discs were exposed from the ventral side and grouped by blocked randomization. In brief, a 2 mm width and 2.5 mm depth lesion was punctured by a custom-made blade (Fig. 8A). Fib-T-G + MSCs group: AF lesion filled with 7 μL Fib-T-G + MSCs adhesive hydrogel and closed carefully by one micro suture (ETHICON 7–0); Fib + MSCs group: AF lesion filled with 7 μL Fib + MSCs adhesive hydrogel and closed by suture as the same; Un-repair control: AF lesion without repair. Intact control: discs exposed without any intervention. All the rats were fed with standardized food, moved freely, and sacrificed at 3 weeks.

2.7.2. Histology and morphology

The samples were harvested and fixed in 10% formalin for 48 h, decalcified with 14% Ethylenediaminetetraacetic Acid (EDTA) for 30 d, and embedded in paraffin wax. The paraffin blocks of discs were cut into 5 μm coronal sections containing the endplate, AF, and NP. The sections were stained with HE for the disc's general morphology. Picrosirius Red staining was used to observe the collagen structure of AF, and the samples were examined and photographed with a microscope (IX73, Olympus, Japan), including polarized light (−) and polarized light (+).

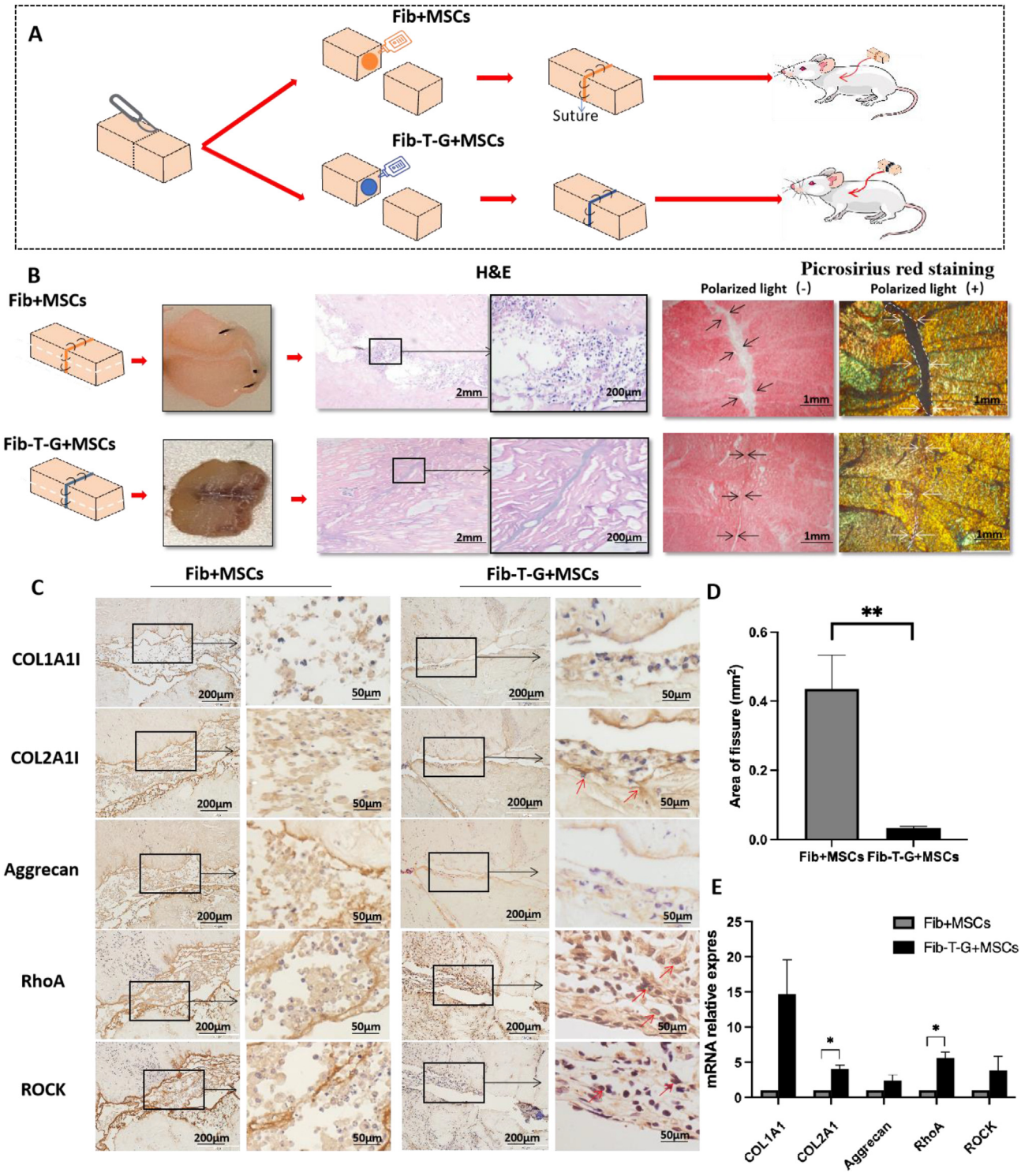

Figure 6. Repair of decellularized AF fissure model (A) Diagram of the experiment of the repair of decellularized AF fissure (B) Hematoxylin and eosin (H&E) and picrosirius red staining (C) Immunohistochemical expression of COL1A1, COL2A1, Aggrecan, RhoA, ROCK (D) The area of fissure was calculated according to the area marked in Picrosirius red staining (E) qPCR analyses of relative expression of genes (COL1A1, COL2A1, Aggrecan, RhoA, ROCK) in Fib + MSCs group and Fib-T-G + MSCs group. The error bars indicate SD. N = 3 (*P < 0.05, **P < 0.01). (For interpretation of the references to colour in this figure legend, the reader is referred to the Web version of this article.)

According to the previous study, the histological score of the degeneration of AF, NP, endplate, and intervertebral disc included eight categories [25]. The histological score ranged from a normal morphology with 0 points to a severe degenerative change with 2 points. The migration and distribution of cells and the morphology of AF were observed in H&E and picrosirius red staining. The calculation of the area of ventral and dorsal AF defect was the same as before. Diaminobenzidine (DAB, ZLI-9018, ZSGB-BIO, China) staining of collagen I, collagen II, and Aggrecan were conducted to evaluate the components of AF under the microscope.

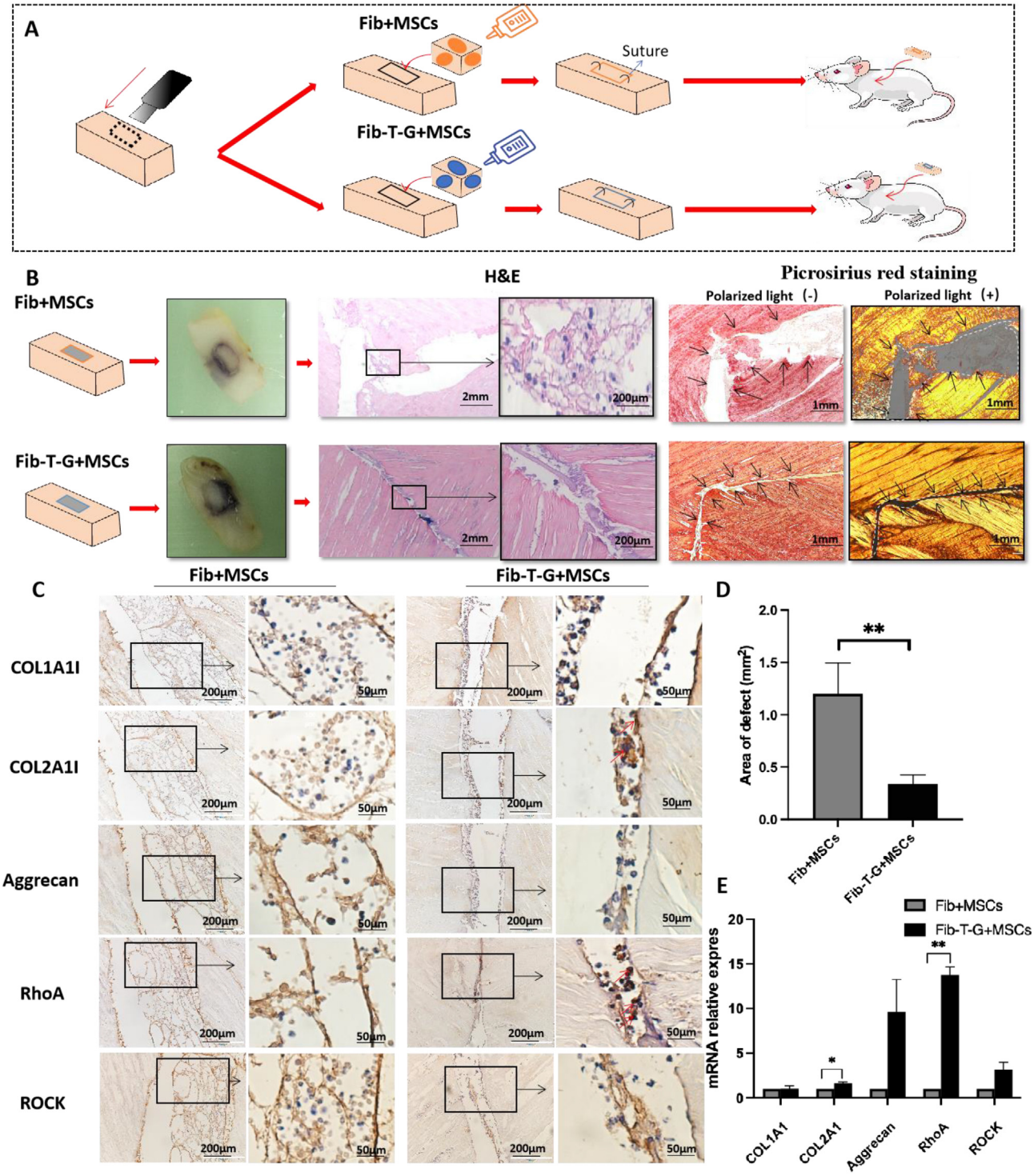

Figure 7. Repair of decellularized AF defect model (A) Diagram of the experiment of the repair of decellularized AF defect (B) Hematoxylin and eosin (H&E) and picrosirius red staining (C) Immunohistochemical expression of COL1A1, COL2A1, Aggrecan, RhoA, ROCK (D) The area of defect was calculated according to the area marked in Picrosirius red staining (E) qPCR analyses of relative expression of genes (COL1A1, COL2A1, Aggrecan, RhoA, ROCK). The error bars indicate SD. N = 3 (*P < 0.05, **P < 0.01). (For interpretation of the references to colour in this figure legend, the reader is referred to the Web version of this article.)

2.8. Statistical analysis

All quantitative data are expressed as the mean ± standard deviation (SD). Differences between the two groups were inspected by using a paired Student's t-test, and a comparison of multiple groups was performed by one-way analysis of variance (ANOVA). The results were considered significant at *P < 0.05, **P < 0.01. All tests were performed with GraphPad Prism 6.0 (GraphPad Software, La Jolla, CA, USA).

3. Results

3.1. Rheological measurements

The viscosity of Fib hydrogel decreased sharply with the increase of

Table 1
Primers sequences used for qPCR analyses.

Name			Product size	NCBI Reference Sequences (Ref Seq)
COL1A1	Sense	GTGCTAAAGGTGCCAATGGT	228	NM_000088.3
	Antisense	CTCCTCGCTTTCCTTCCTCT		
RhoA	Sense	TCGTTAGTCCACGGTCTGGT	116	NM_001313941.2
	Antisense	GCCATTGCTCAGGCAACGAA		
ROCK	Sense	CTGCAACTGGAACTCAACCAAG	100	NM_005406.3
	Antisense	ATTCTTCTACCAATTGCGCTTGC		
Aggrecan	Sense	CCTCTGGACAACCAGGTATTAG	97	NM_001135
	Antisense	CCAGATGTTTCTCCACTCAGAT		
COL2A1	Sense	TCCACGGAAGGCTCCCAGAA	141	NM_001844.5
	Antisense	CCTGCTATTGCCCTCTGCCC		

shear stress, while the viscosity of Fib-T-G hydrogel decreased gradually with the increase of shear stress (Fig. 3C and D). Consistent with that, the shear stress of Fib hydrogel was weak, while the shear stress of Fib hydrogel was strong. At 36 °C and shear rate of 0.04 s^{-1}, Fib-T-G hydrogel showed greater viscosity compared with Fib hydrogel (24.67 ± 1.007 *vs* 459333 ± 169205 mPa s) (Fig. 3E). The above results showed that Fib-T-G hydrogel exhibited better viscosity than Fib hydrogel.

3.2. Tension test

With the increase of force, the strain value gradually increased in the Fib-T-G group, but not in the suture and Fib groups. Generally, the interfacial strain value of the suture group was always zero and the Fib group was almost negligible compared with the Fib-T-G group at loading force of 0.1 N, 0.2 N, 0.3 N and 0.4 N, respectively (Fig. 4C). The Fib-T-G group can better bond the cross-section to resist the loading strain force with broken force at 1.11 ± 0.10 N compared to the suture group at 0 N and the Fib group at 0.12 ± 0.08 N ($P < 0.01$).

3.3. Atomic force microscopy (AFM)

AFM showed that the microstructure of Fib group was loose, while that of Fib-T-G group was tight (Fig. 5E and F). Representative force-displacement and sample modulus for each group demonstrate that Fib-T-G group significantly increased the interfacial stress level and enhanced the modulus of samples, compared with Fib group ($P < 0.01$) (Fig. 5G and H).

3.4. Repair of decellularized AF fissure model

The fissure was connected with continuous collagen fibers in the Fib-T-G + MSCs group, while in the Fib + MSCs group, the fissure was filled with disordered scar tissue in HE staining and picrosirius red staining (Fig. 6B). The gap between the ruptured fibers is counted in picrosirius red staining, with 0.03 ± 0.01 mm^2 in the Fib-T-G + MSCs group, compared to 0.44 ± 0.10 mm^2 in the Fib + MSCs group ($P < 0.01$) (Fig. 6D). The immunohistochemical staining showed that the positive staining area of COL2A1 and RhoA in Fib-T-G + MSCs group was significantly larger than that of Fib + MSCs, while the expressions of COL1A1, Aggrecan, and ROCK showed no significant differences (Fig. 6C). qPCR results also showed that gene expression in Fib-T-G + MSCs group was higher than that in Fib-MSCs group, with the value of COL2A1 (4.02 ± 0.59 *vs* 1, $P < 0.05$) and RhoA (5.60 ± 0.84 *vs* 1, $P < 0.05$) (Fig. 6E). The comprehensive results revealed that Fib-T-G + MSCs adhesive hydrogel showed better repair effect in decellularized AF fissure model.

3.5. Repair of decellularized AF defect model

The defect was connected closely in the Fib-T-G + MSCs group, while in the Fib + MSCs group, the defect was large in HE staining and picrosirius red staining (Fig. 7B). The defect area calculated in picrosirius red staining showed that the Fib-T-G + MSCs group was 0.34 ± 0.09 mm^2, significantly lower than the Fib-T-G + MSCs group's 1.20 ± 0.30 mm^2 ($P < 0.01$) (Fig. 7D). The immunohistochemical staining also showed that the positive staining area of COL2A1 and RhoA in Fib-T-G + MSCs group was significantly larger than that of Fib + MSCs, while the expressions of COL1A1, Aggrecan, and ROCK showed no significant differences (Fig. 7C). The qPCR results showed the same change trend as the fracture model, and the gene expression of Fib-T-G + MSCs group was higher than that of Fib-MSCs group, with the value of COL2A1 (1.66 ± 0.11 *vs* 1, $P < 0.05$) and RhoA (13.78 ± 0.92 *vs* 1, $P < 0.01$) (Fig. 7E). The comprehensive results also revealed that Fib-T-G + MSCs adhesive hydrogel showed better repair effect in decellularized AF defect model.

3.6. Stress stimulation improve the repair effect on annulus fibrosus injury in caudal intervertebral disc of rats

The degree of disc degeneration was more severe in un-repair group and Fib + MSCs group than Fib-T-G + MSCs group in HE staining and picrosirius red staining (Fig. 8B). NP of un-repair group and Fib + MSCs group constituted less than 50% of the disc area, with moderate/severe condensation of the extracellular matrix and few large, rounded cells with intense pericellular matrix staining. However, the NP of Fib-T-G + MSCs group constituted more than 50% of the disc area, maintaining a mild condensation appearance. The distinction between NP and AF could be seen. In addition, severe sclerosis and thickening of the cartilage endplate and chondrocyte clones could be seen in the un-repair group. The cartilage endplate of the Fib + MSCs group also showed some degree of cartilage destruction and chondrocyte clones. In contrast, the cartilage endplate of the Fib-T-G + MSCs group showed mild bony sclerosis and a thin cartilage endplate close to the intack group. The histological score, including NP shape, NP area, NP matrix, NP cellularity, AF/NP border, and AF of Fib-T-G + MSCs group, were significantly lower than those in Fib + MSCs group close to the intack group ($P < 0.01$) (Fig. 8C) In addition, ventral and dorsal AF defects were connected closely in the Fib-T-G + MSCs group, while in the Fib + MSCs group the dorsal AF defect was large in HE staining and picrosirius red staining (Fig. 8B). The area of dorsal AF defect is counted in picrosirius red staining, with 0.02 ± 0.01 mm^2 in the Fib-T-G + MSCs group, compared to 0.13 ± 0.05 mm^2 in the Fib + MSCs group ($P < 0.05$) (Fig. 8D). The immunohistochemical staining showed that the positive staining area of COL2A1 and Aggrecan in Fib-T-G + MSCs group was also significantly larger than that of Fib + MSCs (Fig. 8E). All these results indicated that Fib-T-G + MSCs adhesive hydrogels exhibited excellent repair effects in the rat model of caudal intervertebral disc AF injury, compared with Fib + MSCs, even close to the intack control group.

4. Discussion

Stress plays an important role in the regeneration of musculoskeletal tissue. However, there is limited research on the application of stress stimulation in repairing AF interface damage. In this study, we used an adhesive hydrogel of genipin to repair an AF lesion model representing

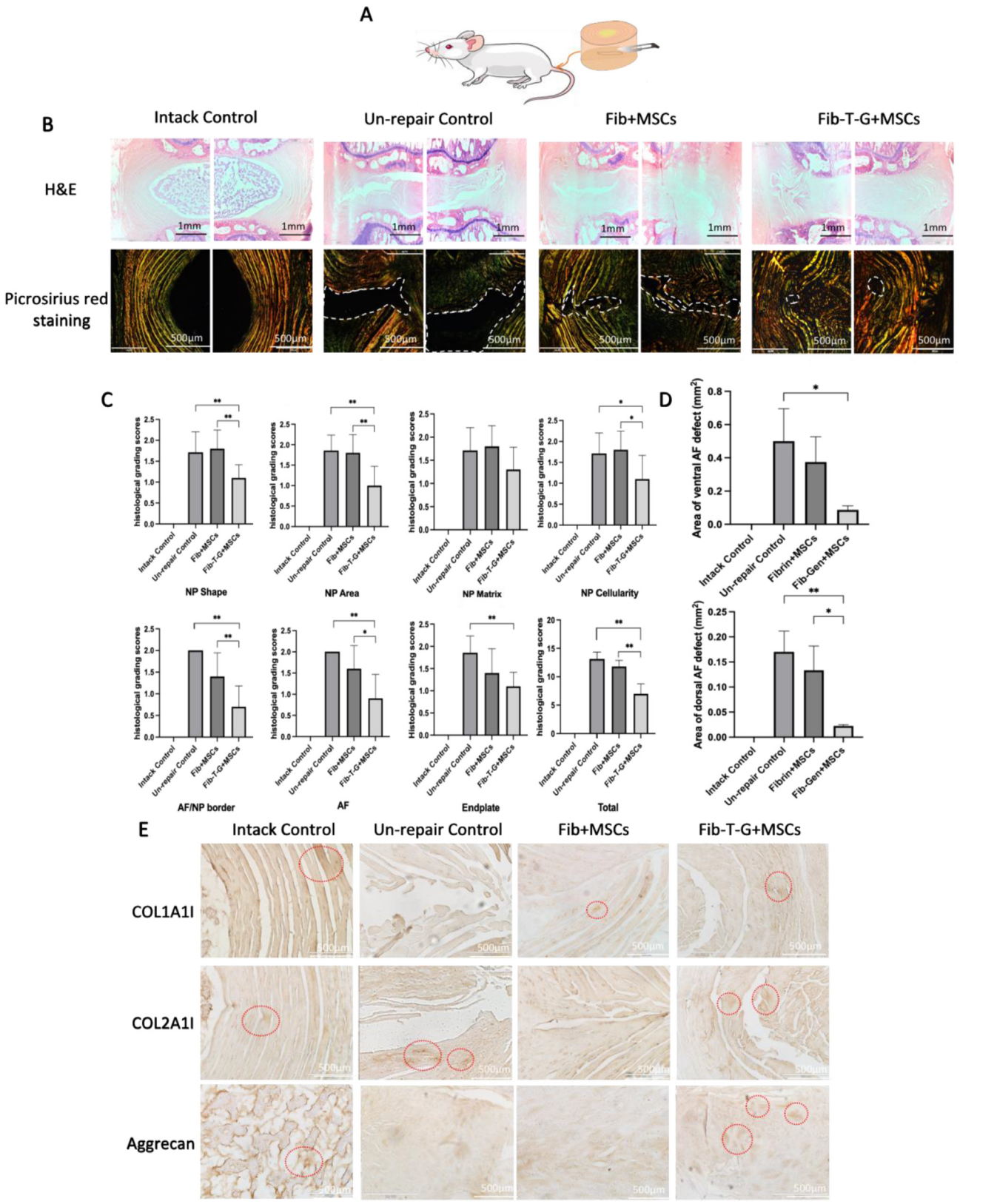

Figure 8. The repair effect on annulus fibrosus injury in caudal intervertebral disc of rats (A) Diagram of the repair effect on annulus fibrosus injury in caudal intervertebral disc of rats (B) Hematoxylin and eosin (H&E) and picrosirius red staining (C) Histological grading scores (D) The area of ventral and dorsal AF defect was calculated according to the area marked in Picrosirius red staining. The error bars indicate SD. N = 3 (*P < 0.05, **P < 0.01) (E) Immunohistochemical expression of COL1A1, COL2A1 in AF and Aggrecan in NP. (For interpretation of the references to colour in this figure legend, the reader is referred to the Web version of this article.)

the repair with stress stimulation and gained a better healing effect than non-adhesive material. The adhesive hydrogel of genipin has better adhesion and can transfer stress stably, as confirmed by interfacial stress experiments. Moreover, the fissure and defect were closely connected, and gene expression activated the mechanical stimulation-related signal pathway. These results revealed that genipin crosslinked hydrogel could bond the interface of AF lesions, transfer stress stably and promote regeneration and repair of AF with the help of stress stimulation.

Under physiological conditions, AF withstands the hydrostatic force caused by disc volume change, in addition to resisting longitudinal compression, tensile force, and axial rotation. And this depends on the AF's stable stress-conduction system. Stress can be felt by fibronectin, which is a collagen-related mechanosensitive matrix component in intervertebral discs regulating collagen reassembly. Moreover, AF cells can also sense stress through stretch-activated ion channels, activated upon cell membrane deformation. Once the structure of AF is damaged, the original stress stimulation pathway is destroyed, inflammatory cells gather, and IVD will be accelerated [22]. Our *in vivo* results of the caudal intervertebral disc of rats are consistent with that: in the un-repair group and non-adhesive repair group, the AF was broken and could not transfer stress in the lesion area, resulting in disordered tissue formation, while in the adhesive repair group, the lesion was connected and could transfer stress stably; thus, the healing resulted with quality collagen fibers formation. Further repair study in the rats also revealed that the adhesive repair eventually slowed down IVD.

Therefore, how to bond the AF section to restore its original stress conduction pathway is the main issue of this study. Since AF needs to withstand multiple loading cycles at high compression, bending, and torsion strength, generating a pressure of 0.1–3 MPa in human beings [26], including its UTS (3.8 MPa), EM (12–24 MPa), and TSF (~65% in a fully flexed position), high requirements are put forward for repair materials. In recent years, with the development of regenerative medicine and tissue engineering technology, the application of stem cell therapy and hydrogels provides a new idea for treating AF injury. Stem cell therapy acts as a seed by secreting cytokines and growth factors that promote the regeneration of AF [27–29]. Among the types of stem cells used for AF repair and regeneration, bone marrow-derived MSCs are the most commonly used stem cells [30,31]. However, how to promote the targeted differentiation of MSCs into AF cells has been a difficult problem. According to the literature, the targeted differentiation of mesenchymal stem cells is related to cell adhesion and stable stress stimulation environment [5,32]. Therefore, selecting suitable materials to provide adequate adhesion and establish a stable environment for stress stimulation is very important.

Hydrogels can seal the defect, transfer stress stably and provide an extracellular matrix environment for seed cell migration [33–35]. In order to better match the physiological characteristics of the AF, hydrogels need to have good bond strength, low biotoxicity, and high failure strain to repair defects successfully without causing stress concentration. The repair ability of a single natural biological hydrogel is very limited. Therefore, in the current study, hydrogels were often crosslinked with other chemical materials [35]. Genipin, which has good adhesion, anti-inflammatory, biocompatibility, and other properties, is often used as a hydrogel crosslinking agent to repair AF injury [36,37]. However, its inability to withstand the daily stress loads of human intervertebral discs makes its practical clinical use difficult. Considering that genipin has a good repair effect, it is still one of the best hydrogel crosslinkers available for AF damage repair strategy. This conclusion coincides with the results of interfacial stress experiment that genipin crosslinked hydrogel enhanced intercellular adhesion and increased the interfacial stress showing good repair potential. Therefore, we attempted to reduce the stress requirements required to close the AF lesion through suture, scaffold, and other external means to help the genipin crosslinked hydrogel to better repair. Inspired by the organ culture technique [10], we used acellular AF scaffolds to make fissure and defect models. The model has the advantages: it can be made and repaired precisely in a sterility bench; large lesion can be made and provides enough material for histological and qPCR investigation; subcutaneous culture provides stress force without worrying about insufficient adhesion strength; only target MSCs in the acellular model, avoiding the interference of the AF cells. In addition, to facilitate the later observation, we chose to fix the adhesive surface with sutures for both groups in the experiment. Moreover, we first repaired the section with hydrogel and fixed it for a period of time before reinforcing it with sutures to avoid stress occlusion.

In simulating the scenario of clinical AF lesions, both the fissure and defect models were investigated in our study, especially in the lesion area. The gap between the fractured section was significantly smaller, with less exogenous cell infiltration in the adhesive repair group than the non-adhesive group. This may be due to adhesive hydrogel bonding to the fractured section tightly, leaving no space for exogenous cells or genipin's anti-inflammatory effect [38]. The MSCs in the lesion secreted significantly more collagen II extracellular matrix, with mechanical stimulation signal RhoA/ROCK gene activated in the adhesive repair group than the non-adhesive group. It is inferred that by maintaining the conduction stress, the stress stimulation signals are transformed into biochemical signals to promote the production of the repair components of the AF.

Our experiments have some limitations. Firstly, the AF lesion model made by acellular scaffolds and the subcutaneous mechanical environment differs from the situation in humans. But to be somewhat, the results indicate mechanical stimulation is very important for AF healing and encourage more efficient adhesive in further study. Secondly, the MSCs may flow out of the lesion area in the non-adhesive repair group, although we sutured the surface of the lesion to keep them. This also affects the accuracy of our observation and comparison of cells to a certain extent. Thirdly, the healing of interfaces is the result of multiple factors. In this experiment, we only focused on the effect of stress stimulation on interfacial healing. In the future, we will conduct further research on the influence of other factors like inflammation on the healing of AF injury.

5. Conclusion

Genipin crosslinked hydrogel can bond the interface of AF lesion and transfer strain force. Stress stimulation maintaining by adhesive hydrogel promotes AF healing.

Author contributions

Zihan Wang[#]: Writing, analysis; Xiaoyu Jin[#]: Experiment; Botao Zhang: Assist in the experiment; Jiaxin Kong: Assist in the experiment; Rongrong Deng: Reviewing; **Ke Wu:** Assist in the experiment; Lin Xie: Reviewing; Xin Liu*: Reviewing and modifying; Ran Kang*: Supervision, guidance and modifying.

Declaration of competing interest

The authors declare no conflict of interests.

Acknowledgement

The research was fund by the National Natural Science of China (81772356), Natural Science Foundation of Jiangsu Province (BK20220464) and Jiangsu Graduate Research and Practice Innovation Program (SJCX22-0838).

References

[1] Mohd Isa IL, Teoh SL, Mohd Nor NH, Mokhtar SA. Discogenic low back pain: anatomy, pathophysiology and treatments of IVD. Int J Mol Sci 2022;24:208. https://doi.org/10.3390/ijms24010208.
[2] Liu C, Jin Z, Ge X, Zhang Y, Xu H. Decellularized annulus fibrosus matrix/chitosan hybrid hydrogels with basic fibroblast growth factor for annulus fibrosus tissue

engineering. Tissue Eng 2019;25:1605–13. https://doi.org/10.1089/ten.TEA.2018.0297.
[3] Guardado AA, Baker A, Weightman A, Hoyland JA, Cooper G. Lumbar intervertebral disc herniation: annular closure devices and key design requirements. Bioeng. Basel Switz. 2022;9:47. https://doi.org/10.3390/bioengineering9020047.
[4] Sun B, Lian M, Han Y, Mo X, Jiang W, Qiao Z, et al. A 3D-bioprinted dual growth factor-releasing intervertebral disc scaffold induces nucleus pulposus and annulus fibrosus reconstruction. Bioact Mater 2021;6:179–90. https://doi.org/10.1016/j.bioactmat.2020.06.022.
[5] Fahey M, Bennett M, Thomas M, Montney K, Vivancos-Koopman I, Pugliese B, et al. MSCs donate mitochondria to articular chondrocytes exposed to mitochondrial, environmental, and mechanical stress. Sci Rep 2022;12:21525. https://doi.org/10.1038/s41598-022-25844-5.
[6] Peng Y, Qing X, Lin H, Huang D, Li J, Tian S, et al. Decellularized disc hydrogels for HBMSCs tissue-specific differentiation and tissue regeneration. Bioact Mater 2021;6:3541–56. https://doi.org/10.1016/j.bioactmat.2021.03.014.
[7] Deng R, Kang R, Jin X, Wang Z, Liu X, Wang Q, et al. Mechanical stimulation promotes MSCs healing the lesion of intervertebral disc annulus fibrosus. Front Bioeng Biotechnol 2023;11:1137199. https://doi.org/10.3389/fbioe.2023.1137199.
[8] Liu X, Sun Y, Chen B, Li Y, Zhu P, Wang P, et al. Novel magnetic silk fibroin scaffolds with delayed degradation for potential long-distance vascular repair. Bioact Mater 2022;7:126–43. https://doi.org/10.1016/j.bioactmat.2021.04.036.
[9] Liu X, Li Y, Sun Y, Chen B, Du W, Li Y, et al. Construction of functional magnetic scaffold with temperature control switch for long-distance vascular injury. Biomaterials 2022;290:121862. https://doi.org/10.1016/j.biomaterials.2022.121862.
[10] Jin X, Kang R, Deng R, Zhao X, Wang Z, Rong W, et al. Fabrication and characterization of an acellular annulus fibrosus scaffold with aligned porous construct for tissue engineering. J Biomater Appl 2022;36:985–95. https://doi.org/10.1177/08853282211041956.
[11] Kang R, Li H, Lysdahl H, Quang Svend Le D, Chen M, Xie L, et al. Cyanoacrylate medical glue application in intervertebral disc annulus defect repair: mechanical and biocompatible evaluation. J Biomed Mater Res B Appl Biomater 2017;105:14–20. https://doi.org/10.1002/jbm.b.33524.
[12] Fujii K, Lai A, Korda N, Hom WW, Evashwick-Rogler TW, Nasser P, et al. Ex-vivo biomechanics of repaired rat intervertebral discs using genipin crosslinked fibrin adhesive hydrogel. J Biomech 2020;113:110100. https://doi.org/10.1016/j.jbiomech.2020.110100.
[13] Kang R, Li H, Xi Z, Ringgard S, Baatrup A, Rickers K, et al. Surgical repair of annulus defect with biomimetic multilamellar nano/microfibrous scaffold in a porcine model: new surgical treatment combining biomimetic, multilamellar nanofibrous scaffold with new closure solution could efficiently close the annulus defect w. J. Tissue Eng. Regen. Med. 2018;12:164–74. https://doi.org/10.1002/term.2384.
[14] Liu X, Zhang Q, Gao G. Solvent-resistant and nonswellable hydrogel conductor toward mechanical perception in diverse liquid media. ACS Nano 2020;14:13709–17. https://doi.org/10.1021/acsnano.0c05932.
[15] Wang Z, Liu H, Luo W, Cai T, Li Z, Liu Y, et al. Regeneration of skeletal system with genipin crosslinked biomaterials. J Tissue Eng 2020;11:2041731420974861. https://doi.org/10.1177/2041731420974861.
[16] Baysan G, Colpankan Gunes O, Akokay P, Husemoglu RB, Ertugruloglu P, Ziylan Albayrak A, et al. Loofah-chitosan and poly (-3-Hydroxybutyrate-Co-3-Hydroxyvalerate) (PHBV) based hydrogel scaffolds for meniscus tissue engineering applications. Int J Biol Macromol 2022;221:1171–83. https://doi.org/10.1016/j.ijbiomac.2022.09.031.
[17] Li Y, Li L, Hölscher C. Therapeutic potential of genipin in central neurodegenerative diseases. CNS Drugs 2016;30:889–97. https://doi.org/10.1007/s40263-016-0369-9.
[18] Song W, Cheng Y, Yan X, Yang S. Long-term study of corneal stroma and endothelium on structure and cells after genipin treatment of rabbit corneas. Transl. Vis. Sci. Technol. 2021;10:9. https://doi.org/10.1167/tvst.10.5.9.
[19] Koudouna E, Huertas-Bello M, Rodriguez CN, Consuelo Henao S, Navarrete ML, Avila MY. Genipin in an ex vivo corneal model of bacterial and fungal keratitis. Transl. Vis. Sci. Technol. 2021;10:31. https://doi.org/10.1167/tvst.10.9.31.
[20] Chen L, Li M, Yang Z, Tao W, Wang P, Tian X, et al. Gardenia jasminoides ellis: ethnopharmacology, phytochemistry, and pharmacological and industrial applications of an important traditional Chinese medicine. J Ethnopharmacol 2020;257:112829. https://doi.org/10.1016/j.jep.2020.112829.
[21] Zhu M, Tan J, Liu L, Tian J, Li L, Luo B, et al. Construction of biomimetic artificial intervertebral disc scaffold via 3D printing and electrospinning. Mater. Sci. Eng. C Mater. Biol. Appl. 2021;128:112310. https://doi.org/10.1016/j.msec.2021.112310.
[22] Peng Y, Huang D, Li J, Liu S, Qing X, Shao Z. Genipin-crosslinked decellularized annulus fibrosus hydrogels induces tissue-specific differentiation of bone mesenchymal stem cells and intervertebral disc regeneration. J. Tissue Eng. Regen. Med. 2020;14:497–509. https://doi.org/10.1002/term.3014.
[23] Ashinsky BG, Gullbrand SE, Bonnevie ED, Mandalapu SA, Wang C, Elliott DM, et al. Multiscale and multimodal structure-function analysis of IVD in a rabbit model. Osteoarthritis Cartilage 2019;27:1860–9. https://doi.org/10.1016/j.joca.2019.07.016.
[24] Li Q, Qu F, Han B, Wang C, Li H, Mauck RL, et al. Micromechanical anisotropy and heterogeneity of the meniscus extracellular matrix. Acta Biomater 2017;54:356–66. https://doi.org/10.1016/j.actbio.2017.02.043.
[25] Tomaszewski KA, Henry BM, Gładysz T, Głowacki R, Walocha JA, Tomaszewska R. Validation of the intervertebral disc histological degeneration score in cervical intervertebral discs and their end plates. Spine J. Off. J. North Am. Spine Soc. 2017;17:738–45. https://doi.org/10.1016/j.spinee.2017.01.006.
[26] Bowles RD, Setton LA. Biomaterials for intervertebral disc regeneration and repair. Biomaterials 2017;129:54–67. https://doi.org/10.1016/j.biomaterials.2017.03.013.
[27] Widjaja G, Jalil AT, Budi HS, Abdelbasset WK, Efendi S, Suksatan W, et al. Mesenchymal stromal/stem cells and their exosomes application in the treatment of intervertebral disc disease: a promising frontier. Int Immunopharm 2022;105:108537. https://doi.org/10.1016/j.intimp.2022.108537.
[28] Yuan Q, Wang X, Liu L, Cai Y, Zhao X, Ma H, et al. Exosomes derived from human placental MSCs carrying AntagomiR-4450 alleviate IVD through upregulation of ZNF121. Stem Cell Dev 2020;29:1038–58. https://doi.org/10.1089/scd.2020.0083.
[29] Zhu L, Shi Y, Liu L, Wang H, Shen P, Yang H. Mesenchymal stem cells-derived exosomes ameliorate nucleus pulposus cells apoptosis via delivering MiR-142-3p: therapeutic potential for intervertebral disc degenerative diseases. Cell Cycle Georget. Tex 2020;19:1727–39. https://doi.org/10.1080/15384101.2020.1769301.
[30] Hu Y-C, Zhang X-B, Lin M-Q, Zhou H-Y, Cong M-X, Chen X-Y, et al. Nanoscale treatment of IVD: MSCs exosome transplantation. Curr Stem Cell Res Ther 2023;18:163–73. https://doi.org/10.2174/1574888X17666220422093103.
[31] Bhujel B, Shin H-E, Choi D-J, Han I. Mesenchymal stem cell-derived exosomes and intervertebral disc regeneration: review. Int J Mol Sci 2022;23:7306. https://doi.org/10.3390/ijms23137306.
[32] Halim A, Ariyanti AD, Luo Q, Song G. Recent progress in engineering mesenchymal stem cell differentiation. Stem Cell Rev. Rep. 2020;16:661–74. https://doi.org/10.1007/s12015-020-09979-4.
[33] Hasani-Sadrabadi MM, Sarrion P, Pouraghaei S, Chau Y, Ansari S, Li S, et al. An engineered cell-laden adhesive hydrogel promotes craniofacial bone tissue regeneration in rats. Sci Transl Med 2020;12:eaay6853. https://doi.org/10.1126/scitranslmed.aay6853.
[34] Tang Q, Lu B, He J, Chen X, Fu Q, Han H, et al. Exosomes-loaded thermosensitive hydrogels for corneal epithelium and stroma regeneration. Biomaterials 2022;280:121320. https://doi.org/10.1016/j.biomaterials.2021.121320.
[35] Borelli AN, Young MW, Kirkpatrick BE, Jaeschke MW, Mellett S, Porter S, et al. Stress relaxation and composition of hydrazone-crosslinked hybrid biopolymer-synthetic hydrogels determine spreading and secretory properties of MSCs. Adv. Healthc. Mater. 2022;11:e2200393. https://doi.org/10.1002/adhm.202200393.
[36] Panebianco CJ, Rao S, Hom WW, Meyers JH, Lim TY, Laudier DM, et al. Genipin-crosslinked fibrin seeded with oxidized alginate microbeads as a novel composite biomaterial strategy for intervertebral disc cell therapy. Biomaterials 2022;287:121641. https://doi.org/10.1016/j.biomaterials.2022.121641.
[37] Zheng Y, Xu G, Ni Q, Wang Y, Gao Q, Zhang Y. Microemulsion delivery system improves cellular uptake of genipin and its protective effect against aβ1-42-induced PC12 cell cytotoxicity. Pharmaceutics 2022;14:617. https://doi.org/10.3390/pharmaceutics14030617.
[38] Fan X, Lin L, Cui B, Zhao T, Mao L, Song Y, et al. Therapeutic potential of genipin in various acute liver injury, fulminant hepatitis, NAFLD and other non-cancer liver diseases: more friend than foe. Pharmacol Res 2020;159:104945. https://doi.org/10.1016/j.phrs.2020.104945.